International Journal of Applied Mechanics
Vol. 2, No. 1 (2010) 117–143

DOI: 10.1142/S1758825110000500

Imperial College Press
www.icpress.co.uk

# REFINED BEAM THEORIES BASED ON A UNIFIED FORMULATION

ERASMO CARRERA

*Aeronautic and Space Engineering Department*
*24 c.so Duca degli Abruzzi, Politecnico di Torino*
*10129, Turin, Italy*

GAETANO GIUNTA*

*Advanced Materials and Structures Department*
*29 av. John F. Kennedy*
*Centre de Recherche Public Henri Tudor*
*L-1855, Luxembourg-Kirchberg, Luxembourg*
*gaetano.giunta@tudor.lu*

Received 20 April 2009
Accepted 19 August 2009

This paper proposes several axiomatic refined theories for the linear static analysis of beams made of isotropic materials. A hierarchical scheme is obtained by extending plates and shells Carrera's Unified Formulation (CUF) to beam structures. An $N$-order approximation via Mac Laurin's polynomials is assumed on the cross-section for the displacement unknown variables. $N$ is a free parameter of the formulation. Classical beam theories, such as Euler-Bernoulli's and Timoshenko's, are obtained as particular cases. According to CUF, the governing differential equations and the boundary conditions are derived in terms of a fundamental nucleo that does not depend upon the approximation order. The governing differential equations are solved via the Navier type, closed form solution. Rectangular and I-shaped cross-sections are accounted for. Beams undergo bending and torsional loadings. Several values of the span-to-height ratio are considered. Slender as well as deep beams are analysed. Comparisons with reference solutions and three-dimensional FEM models are given. The numerical investigation has shown that the proposed unified formulation yields the complete three-dimensional displacement and stress fields for each cross-section as long as the appropriate approximation order is considered. The accuracy of the solution depends upon the geometrical parameters of the beam and loading conditions.

*Keywords*: Beam structures; Hierarchical modelling; Closed form solution.

## 1. Introduction

Many primary and secondary structural elements, such as aircraft wings, helicopter rotor blades, robot arms or structures in civil construction, can be idealised as beams. An accurate prediction of the mechanics of beams plays a paramount role

*Corresponding author

in their correct, safe and optimal design and utilisation. Engineering fields, such as Aeronautics, characterised by high levels of technology also require more and more accurate models. Beam modelling therefore represents an important topic of research.

Euler-Bernoulli's (EB) and Timoshenko's (TB) (see [Timoshenko, 1921], [Timoshenko, 1922] and [Timoshenko and Goodier, 1970]) theories represent the classical one-dimensional models (CMs) for the bending analysis of beam structures made of isotropic materials. The cross-section is considered to be rigid on its plane. EB discards the shear deformation while TB accounts for a constant value. Material stiffness coefficients should be opportunely reduced. As the beam becomes less and less slender, its mechanics is more and more three-dimensional and CMs do not yield accurate results. The accuracy also depends on the material properties and the cross-sectional geometry. In the case of I-shaped cross-sections, non-classical deformations are important for the global elastic behaviour of the beam. As far as torsional problems are concerned, Saint-Venant's and Prandtl's models represent the classical solutions. Saint-Venant [1855] postulated the displacement field assuming that the deformation of a twisted shaft consists of a rigid rotation, as in the case of a circular cross-section and a warping that is constant along the beam axis. Prandtl [1903] introduced the membrane analogy for the study of torsion: the problem is reduced to the study of a homogeneous membrane supported at the edges, with the same outline as the beam cross-section and subjected to a uniform tension at the edges and a uniform transverse bending pressure. Improvements in CMs have been proposed to account for non-classical effects and non-conventional materials. Some of them are discussed hereafter. Stephen and Levinson [1979] accounted for a linear variation of the shear deformation. Within the framework of the finite element method, Kant and Manjunath [1989] proposed kinematic fields with a second- and a third-order variation of the longitudinal displacement. The transversal displacement is constant. Beams made of composite and sandwich materials were investigated. These authors accounted for a linear variation of the transversal displacement in [Kant and Manjunath, 1990]. Models with quadratic and cubic variation were addressed in [Manjunath and Kant, 1993]. Transverse stresses were computed via the integration of the indefinite equilibrium equations through three different numerical techniques: the direct integration method, the forward and central direct finite difference method and the exact curve fitting method. Vinayak *et al.* [1996] and Prathap *et al.* [1996] proposed a theory for composite beams in which the longitudinal displacement is a cubic function of the coordinate transversal to the axis of the beam, while the transversal displacement varies quadratically. Rand [1998] formulated a model with five degrees of freedom: three cross-sectional displacements, a twist angle, which are constant above the cross-section, and a three-dimensional warping function. Solid and thin-walled beams made of composite materials were investigated. The author addressed the importance of the warping function in [Rand, 2000]. Sinus finite elements were proposed by Ganapathi *et al.* [1999] to study sandwich beams

that account for transverse shear and warping. Starting from that work, Vidal and Polit [2008] developed a family of finite elements considering a Heaviside function or the double superposition hypothesis by Li and Liu [1997]. Laminated rectangular beams were analysed. Gjelsvik [1981] presented an isotropic beam theory in which the beam is split into plate segments. The continuity of the displacements is imposed via geometric considerations, while global and local equilibrium is obtained through the principle of virtual work. Wagner and Gruttmann [2002] formulated a prismatic beam model to study flexural shear stresses in thin-walled isotropic composite beams undergoing torsionless bending. Estivalezes and Barrau [1998], using a homogenisation method, formulated a simplified calculation method applicable to a box beam made of orthotropic materials whose axis is non-orthogonal to the beam cross-section. Lee and Lee [2004] proposed an analytical model of I-shaped composite beams that accounts for flexural-torsional behaviour. Lee [2005] enhanced that model by incorporating transverse shear deformation. Stemming from the work by Berdichevsky [1976], Yu *et al.* [2002] adopted a variational-asymptotic approach for the Timoshenko-like modelling of initially curved and twisted composite beams. Thanks to that approach, no "ad hoc" assumptions on the main unknown are adopted and the general, three-dimensional, anisotropic, elasticity problem is decoupled into a linear, two-dimensional, cross-section analysis (in order to obtain the cross-section stiffness matrix) and a non-linear, one-dimensional beam analysis. The Timoshenko-like model was then obtained by reproducing the three-dimensional strain energy in terms of one-dimensional strain terms. Classical TB model is enhanced in the sense that in- and out-of-plane waring are accounted for. The method was applied for the derivation of an analytical closed form solution for isotropic prismatic beams by Yu and Hodges [2004]. That solution was compared to the elasticity one. It was also applied to the modelling of composite rotor blades of wind turbines (see [Hodges and Yu, 2007]). Liu and Zhang [2009] investigated the static response and the free vibration of a cantilever beam via a strain-constructed point interpolation method. Kapania and Raciti [1989a, 1989b] presented a literature review of the developments in laminated beams and plates models for static, buckling, free-vibration and wave propagation analysis. Another review on significant advances in composite beams modelling was written by Hodges [1990].

The present paper proposes a systemic manner of formulating axiomatically refined beam models. Via a concise notation for the kinematic field, the governing differential equations and the corresponding boundary conditions are reduced to a 'fundamental nucleo' in terms of the displacement components. The fundamental nucleo does not depend upon the approximation order. It is, therefore, assumed as free parameter of the formulation. This scheme is named Carrera's Unified Formulation and it was previously applied to the modelling of anisotropic plate and shell structures (see [Carrera, 2003]). Displacement-based theories that account for non-classical effects, such as transverse shear, in- and out-of-plane warping of the cross-section, can be formulated. It is worth mentioning that no special warping

functions need to be assumed. Classical models, such as EB and TB, can be retrieved as particular cases. Navier's, closed form solution is adopted to solve the governing differential equations. Slender and deep beams are investigated. The cross-section is considered to be rectangular or I-shaped. Beams are subjected to bending or torsional loadings. The proposed models are validated towards reference exact solutions or three-dimensional FEM models.

## 2. Preliminaries

A beam is a structure whose axial extension, $l$, is predominant compared to any other dimension orthogonal to it. The cross-section, $\Omega$, is identified by intersecting the beam with planes that are orthogonal to its axis. Cross-sections that are obtainable by the union of $N_{\Omega^k}$ rectangular sub-domains

$$\Omega = \bigcup_{k=1}^{N_{\Omega^k}} \Omega^k, \tag{2.1}$$

with

$$\Omega^k = \{(x, y) : x_1^k \leq x \leq x_2^k; y_1^k \leq y \leq y_2^k\}. \tag{2.2}$$

are considered, $\{(x_i^k, y_j^k) : i, j = 1, 2\}$ being the coordinates of the corner points of each $k$ sub-domain. Through the paper, superscript '$k$' represents the cross-section sub-domain index, while as subscript it stands for summation over the range $(1, N_{\Omega^k})$. Figures 1(a) and 1(b) present the geometrical data of a rectangular and an I-shaped cross-section. The reference system is also shown there: $x$ and $y$ axes are two orthogonal directions laying on the cross-section. The $z$ coordinate is coincident

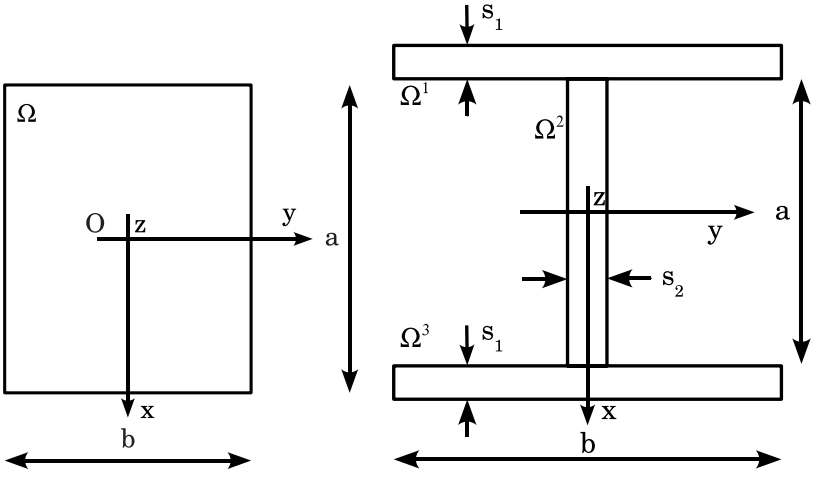


(a) (b)

Fig. 1. Reference system and geometry of (a) a rectangular and (b) an I-shaped cross-section.

to the axis of the beam. It is bounded such that $0 \leq z \leq l$. The cross-section is considered constant along $z$. The displacement field is

$$\mathbf{u}(x,y,z) = \begin{Bmatrix} u_x(x,y,z) \\ u_y(x,y,z) \\ u_z(x,y,z) \end{Bmatrix}, \tag{2.3}$$

in which $u_x$, $u_y$, and $u_z$ are the displacement components along the $x$, $y$, and $z$ axes. The stress, $\boldsymbol{\sigma}$, and strain, $\boldsymbol{\varepsilon}$, vectors are grouped into vectors $\boldsymbol{\sigma}_n$, $\boldsymbol{\varepsilon}_n$ that lay on the cross-section

$$\boldsymbol{\sigma}_n = \begin{Bmatrix} \sigma_{xz} \\ \sigma_{yz} \\ \sigma_{zz} \end{Bmatrix}, \quad \boldsymbol{\varepsilon}_n = \begin{Bmatrix} \varepsilon_{xz} \\ \varepsilon_{yz} \\ \varepsilon_{zz} \end{Bmatrix}, \tag{2.4}$$

and $\boldsymbol{\sigma}_p$, $\boldsymbol{\varepsilon}_p$ laying on planes orthogonal to $\Omega$

$$\boldsymbol{\sigma}_p = \begin{Bmatrix} \sigma_{xx} \\ \sigma_{yy} \\ \sigma_{xy} \end{Bmatrix}, \quad \boldsymbol{\varepsilon}_p = \begin{Bmatrix} \varepsilon_{xx} \\ \varepsilon_{yy} \\ \varepsilon_{xy} \end{Bmatrix}. \tag{2.5}$$

In the case of small displacements with respect to a characteristic dimension of $\Omega$, linear relations between strain and displacement components hold

$$\boldsymbol{\varepsilon}_n = \begin{Bmatrix} u_{x,z} + u_{z,x} \\ u_{y,z} + u_{z,y} \\ u_{z,z} \end{Bmatrix}, \quad \boldsymbol{\varepsilon}_p = \begin{Bmatrix} u_{x,x} \\ u_{y,y} \\ u_{x,y} + u_{y,x} \end{Bmatrix}. \tag{2.6}$$

Subscripts '$x$', '$y$' and '$z$' when preceded by comma represent derivation versus the spatial coordinates. A compact vectorial notation can be adopted for Eqs. (2.6)

$$\boldsymbol{\varepsilon}_n = \mathbf{D}_{np}\mathbf{u} + \mathbf{D}_{nz}\mathbf{u}, \quad \boldsymbol{\varepsilon}_p = \mathbf{D}_p\mathbf{u}, \tag{2.7}$$

where $\mathbf{D}_{np}$, $\mathbf{D}_{nz}$, and $\mathbf{D}_p$ are the following differential matrix operators

$$\mathbf{D}_{np} = \begin{bmatrix} 0 & 0 & \frac{\partial}{\partial x} \\ 0 & 0 & \frac{\partial}{\partial y} \\ 0 & 0 & 0 \end{bmatrix}, \quad \mathbf{D}_{nz} = \begin{bmatrix} \frac{\partial}{\partial z} & 0 & 0 \\ 0 & \frac{\partial}{\partial z} & 0 \\ 0 & 0 & \frac{\partial}{\partial z} \end{bmatrix}, \quad \mathbf{D}_p = \begin{bmatrix} \frac{\partial}{\partial x} & 0 & 0 \\ 0 & \frac{\partial}{\partial y} & 0 \\ \frac{\partial}{\partial y} & \frac{\partial}{\partial x} & 0 \end{bmatrix}. \tag{2.8}$$

In the case of beams made of linear elastic materials, the generalised Hooke law holds. Its compact vectorial form is

$$\boldsymbol{\sigma} = \mathbf{C}\boldsymbol{\varepsilon}. \tag{2.9}$$

According to Eqs. (2.4) and (2.5), Eq. (2.9) reads

$$\begin{aligned} \boldsymbol{\sigma}_p &= \mathbf{C}_{pp}\boldsymbol{\varepsilon}_p + \mathbf{C}_{pn}\boldsymbol{\varepsilon}_n, \\ \boldsymbol{\sigma}_n &= \mathbf{C}_{np}\boldsymbol{\varepsilon}_p + \mathbf{C}_{nn}\boldsymbol{\varepsilon}_n. \end{aligned} \tag{2.10}$$

Matrixes $\mathbf{C}_{pp}$, $\mathbf{C}_{np}$ and $\mathbf{C}_{nn}$ are

$$\mathbf{C}_{pp} = \begin{bmatrix} C_{11} & C_{12} & 0 \\ C_{12} & C_{22} & 0 \\ 0 & 0 & C_{66} \end{bmatrix}, \quad \mathbf{C}_{pn} = \mathbf{C}_{np}^T = \begin{bmatrix} 0 & 0 & C_{13} \\ 0 & 0 & C_{23} \\ 0 & 0 & 0 \end{bmatrix},$$
$$\mathbf{C}_{nn} = \begin{bmatrix} C_{55} & 0 & 0 \\ 0 & C_{44} & 0 \\ 0 & 0 & C_{33} \end{bmatrix}. \tag{2.11}$$

Superscript '$T$' represents the transposition operator. For the sake of brevity, the dependency of the coefficients $C_{ij}$ versus Young's moduli and Poisson's ratios is not reported. It can be found in [Tsai, 1988] or [Reddy, 2004].

## 3. Refined Beam Theories

The variation of the main unknowns towards $x$ and $y$ axes can be postulated a-priori, since the cross-section is negligible compared to the axial extension of the beam. Several displacement-based theories can be formulated on the basis of the following generic kinematic field

$$\mathbf{u}(x, y, z) = F_\tau(x, y)\mathbf{u}_\tau(z), \quad \text{with } \tau = 1, 2, \ldots, N_u = N_u(N). \tag{3.1}$$

$N_u$ stands for the number of unknowns. It depends on the approximation order $N$ that is a free parameter of the formulation. The compact expression is based on Einstein's notation: repeated subscript $\tau$ indicates summation. Thanks to this notation, problem's governing differential equations and boundary conditions can be derived in a unified manner, that is, in terms of a single 'fundamental nucleo'. In such a manner, the complexity related to higher than classical approximation terms is tackled and the theoretical formulation is valid for the generic approximation order and approximating functions $F_\tau(x, y)$. Among the various manner to interpolate the displacement field, functions $F_\tau$ are assumed to be Mac Laurin's polynomials. This choice is inspired by the classical beam models. Table 1 presents $N_u$ and

Table 1. Mac Laurin's polynomials.

| $N$ | $N_u$ | $F_\tau$ |
|---|---|---|
| 0 | 1 | $F_1 = 1$ |
| 1 | 3 | $F_2 = x \quad F_3 = y$ |
| 2 | 6 | $F_4 = x^2 \quad F_5 = xy \quad F_6 = y^2$ |
| 3 | 10 | $F_7 = x^3 \quad F_8 = x^2y \quad F_9 = xy^2 \quad F_{10} = y^3$ |
| ... | ... | ... |
| $N$ | $\frac{(N+1)(N+2)}{2}$ | $F_{\frac{N^2+N+2}{2}} = x^N \quad F_{\frac{N^2+N+4}{2}} = x^{N-1}y \quad \ldots$ |
| | | $F_{\frac{N(N+3)}{2}} = xy^{N-1} \quad F_{\frac{(N+1)(N+2)}{2}} = y^N$ |

$F_\tau$ as functions of $N$. The actual governing differential equations and boundary conditions due to a fixed approximation order and polynomials' type are obtained straightforwardly via summation of the nucleo corresponding to each term of the expansion. According to the previous choice of polynomial function, the generic, $N$-order displacement field is

$$\begin{aligned} u_x &= u_{x1} + u_{x2}x + u_{x3}y + \cdots + u_{x\frac{(N^2+N+2)}{2}}x^N + \cdots + u_{x\frac{(N+1)(N+2)}{2}}y^N, \\ u_y &= u_{y1} + u_{y2}x + u_{y3}y + \cdots + u_{y\frac{(N^2+N+2)}{2}}x^N + \cdots + u_{y\frac{(N+1)(N+2)}{2}}y^N, \\ u_z &= u_{z1} + u_{z2}x + u_{z3}y + \cdots + u_{z\frac{(N^2+N+2)}{2}}x^N + \cdots + u_{z\frac{(N+1)(N+2)}{2}}y^N. \end{aligned} \tag{3.2}$$

As far as the first-order approximation order is concerned, its kinematic field is obtained as particular case of Eqs. (3.2)

$$\begin{aligned} u_x &= u_{x1} + u_{x2}x + u_{x3}y, \\ u_y &= u_{y1} + u_{y2}x + u_{y3}y, \\ u_z &= u_{z1} + u_{z2}x + u_{z3}y. \end{aligned} \tag{3.3}$$

Classical beam models, such as TB

$$\begin{aligned} u_x &= u_{x1}, \\ u_y &= u_{y1}, \\ u_z &= u_{z1} + u_{z2}x + u_{z3}y \end{aligned} \tag{3.4}$$

and EB

$$\begin{aligned} u_x &= u_{x1}, \\ u_y &= u_{y1}, \\ u_z &= u_{z1} - u_{x1,z}x - u_{y1,z}y, \end{aligned} \tag{3.5}$$

can be derived straightforwardly from a first-order approximation model. Degrees of freedom $\{u_{ij} : i = x, y;\ j = 2, 3\}$ are discarded via a numerical penalisation technique derived from the finite element method: the diagonal term of the stiffness matrix corresponding to a degree of freedom that has to be discarded is set equal to a value three order of magnitude higher than the maximum value of the stiffness matrix. Also for EB, shear deformation is neglected via penalisation, in the same manner, of material shear stiffness coefficients $C_{44}$ and $C_{55}$. In TB, no shear correction coefficient is considered, since it depends upon several parameters, such as the geometry of the cross-section (see [Cowper, 1966] and [Murty, 1970]). Higher orders models yield a more detailed description of the shear mechanics (no shear correction coefficient is required), the transverse to the section deformations, the coupling of the spatial directions due to Poisson's effect and the torsional mechanics than classical models do. EB theory neglects them all, since it

was formulated to describe the bending mechanics. TB model accounts for constant shear stress and strain components. In the case of classical models and first-order approximation, the material stiffness coefficients $C_{ij}$ in Eqs. (2.11) should be corrected in order to contrast a phenomenon known in literature as Poisson's locking (see [Carrera and Brischetto, 2008a and 2008b]). This correction is presented in Appendix A.

## 4. Governing Differential Equations

The strong form of the governing differential equations and the boundary conditions are obtained in terms of the displacement components and their derivatives through the Principle of Virtual Displacements (PVD)

$$\delta L_i = \delta L_p + \delta L_l. \tag{4.1}$$

$L_i$ represents the strain energy. $L_p$ and $L_l$ stand for the work due to a surface loading, $\mathbf{p}^k$, and a line loading, $\mathbf{l}^k$ that act on a $k$ sub-domain. $\delta$ stands for a virtual variation.

### 4.1. *Variation of the strain energy*

According to the grouping of the stress and strain components in Eqs. (2.4) and (2.5), the virtual variation of the strain energy is considered as sum of two contributes

$$\delta L_i = \int_l \int_\Omega \delta \boldsymbol{\epsilon}_n^T \boldsymbol{\sigma}_n \, d\Omega \, dz + \int_l \int_\Omega \delta \boldsymbol{\epsilon}_p^T \boldsymbol{\sigma}_p \, d\Omega \, dz. \tag{4.2}$$

By substitution of the geometrical relations, Eqs. (2.7), the material constitutive equations, Eqs. (2.10), and the unified hierarchical approximation of the displacements, Eq. (3.1), and after integration by parts, Eq. (4.2) reads

$$\begin{aligned}
\delta L_i = \int_l \delta \mathbf{u}_\tau^T \int_\Omega [ & -\mathbf{D}_{nz}^T \mathbf{C}_{np} F_\tau (\mathbf{D}_p F_s \mathbf{I}) - \mathbf{D}_{nz}^T \mathbf{C}_{nn} F_\tau (\mathbf{D}_{np} F_s \mathbf{I}) - \mathbf{D}_{nz}^T \mathbf{C}_{nn} F_\tau F_s \mathbf{D}_{nz} \\
& + (\mathbf{D}_{np} F_\tau \mathbf{I})^T \mathbf{C}_{np} (\mathbf{D}_p F_s \mathbf{I}) + (\mathbf{D}_{np} F_\tau \mathbf{I})^T \mathbf{C}_{nn} (\mathbf{D}_{np} F_s \mathbf{I}) + (\mathbf{D}_{np} F_\tau \mathbf{I})^T \mathbf{C}_{nn} F_s \mathbf{D}_{nz} \\
& + (\mathbf{D}_p F_\tau \mathbf{I})^T \mathbf{C}_{pp} (\mathbf{D}_p F_s \mathbf{I}) + (\mathbf{D}_p F_\tau \mathbf{I})^T \mathbf{C}_{pn} (\mathbf{D}_{np} F_s \mathbf{I}) + (\mathbf{D}_p F_\tau \mathbf{I})^T \mathbf{C}_{pn} F_s \mathbf{D}_{nz}] \\
& \times d\Omega \, \mathbf{u}_s \, dz + \delta \mathbf{u}_\tau^T \int_\Omega F_\tau [\mathbf{C}_{np} (\mathbf{D}_p F_s \mathbf{I}) + \mathbf{C}_{nn} (\mathbf{D}_{np} F_s \mathbf{I}) + \mathbf{C}_{nn} F_s \mathbf{D}_{nz}] \\
& \times d\Omega \, \mathbf{u}_s |_{z=0}^{z=l}.
\end{aligned} \tag{4.3}$$

$\mathbf{I}$ is the unit matrix. The virtual variation of the strain energy in a compact vectorial form is

$$\delta L_i = \int_l \delta \mathbf{u}_\tau^T \, \mathbf{K}^{\tau s} \, \mathbf{u}_s \, dz + \delta \mathbf{u}_\tau^T \, \mathbf{\Pi}^{\tau s} \, \mathbf{u}_s |_{z=0}^{z=l}. \tag{4.4}$$

The components of the differential matrix $\mathbf{K}^{\tau s}$ are

$$
\begin{gathered}
K_{xx}^{\tau s} = C_{11} E_{\tau,_x s,_x} + C_{66} E_{\tau,_y s,_y} - C_{55} E_{\tau s} \frac{\partial^2}{\partial z^2}, \\
K_{yy}^{\tau s} = C_{22} E_{\tau,_y s,_y} + C_{66} E_{\tau,_x s,_x} - C_{44} E_{\tau s} \frac{\partial^2}{\partial z^2}, \\
K_{zz}^{\tau s} = C_{44} E_{\tau,_y s,_y} + C_{55} E_{\tau,_x s,_x} - C_{33} E_{\tau s} \frac{\partial^2}{\partial z^2}, \\
K_{xy}^{\tau s} = C_{12} E_{\tau,_x s,_y} + C_{66} E_{\tau,_y s,_x}, \quad K_{yx}^{\tau s} = C_{12} E_{\tau,_y s,_x} + C_{66} E_{\tau,_x s,_y}, \\
K_{xz}^{\tau s} = (C_{13} E_{\tau,_x s} - C_{55} E_{\tau s,_x}) \frac{\partial}{\partial z}, \quad K_{zx}^{\tau s} = -(C_{13} E_{\tau s,_x} - C_{55} E_{\tau,_x s}) \frac{\partial}{\partial z}, \\
K_{yz}^{\tau s} = (C_{23} E_{\tau,_y s} - C_{44} E_{\tau s,_y}) \frac{\partial}{\partial z}, \quad K_{zy}^{\tau s} = -(C_{23} E_{\tau s,_y} - C_{44} E_{\tau,_y s}) \frac{\partial}{\partial z}.
\end{gathered}
\tag{4.5}
$$

Terms $\{E_{\tau,_\phi s,_\xi} : \phi, \xi = x, y\}$, $\{E_{\tau,_\phi s} : \phi = x, y\}$, $\{E_{\tau s,_\phi} : \phi = x, y\}$ and $E_{\tau s}$ are the cross-section inertial momenta

$$
\begin{gathered}
E_{\tau,_\phi s,_\xi} = \left( \int_{\Omega^k} F_{\tau,_\phi} F_{s,_\xi} \, d\Omega \right)_k, \quad E_{\tau s} = \left( \int_{\Omega^k} F_\tau F_s \, d\Omega \right)_k, \\
E_{\tau,_\phi s} = \left( \int_{\Omega^k} F_{\tau,_\phi} F_s \, d\Omega \right)_k, \quad E_{\tau s,_\phi} = \left( \int_{\Omega^k} F_\tau F_{s,_\phi} \, d\Omega \right)_k.
\end{gathered}
\tag{4.6}
$$

Their analytical solution is presented in appendix B. As far as the boundary conditions are concerned, the components of $\mathbf{\Pi}^{\tau s}$ are

$$
\begin{gathered}
\Pi_{xx}^{\tau s} = C_{55} E_{\tau s} \tfrac{\partial}{\partial z}, \quad \Pi_{yy}^{\tau s} = C_{44} E_{\tau s} \tfrac{\partial}{\partial z}, \quad \Pi_{zz}^{\tau s} = C_{33} E_{\tau s} \tfrac{\partial}{\partial z}, \\
\Pi_{xy}^{\tau s} = \Pi_{yx}^{\tau s} = 0, \quad \Pi_{xz}^{\tau s} = C_{55} E_{\tau s,_x}, \quad \Pi_{yz}^{\tau s} = C_{44} E_{\tau s,_y}, \\
\Pi_{zx}^{\tau s} = C_{13} E_{\tau s,_x}, \quad \Pi_{zy}^{\tau s} = C_{23} E_{\tau s,_y}.
\end{gathered}
\tag{4.7}
$$

### 4.2. *Virtual work of the external loadings*

The virtual work done by the external loadings is assumed to be due to a surface loading and a line loading.

#### 4.2.1. *Surface loading*

The components of a surface loading are

$$
\mathbf{p}^{kT} = \{ p_{xx}^{k\pm} \quad p_{yy}^{k\pm} \quad p_{xy}^{k\pm} \quad p_{yx}^{k\pm} \quad p_{xz}^{k\pm} \quad p_{yz}^{k\pm} \}. \tag{4.8}
$$

They act as shown in Fig. 2. The lateral surfaces $\{S_\phi^{k\pm} : \phi = x, y\}$ of the beam are defined on the basis of the normal versor $\{n_\phi^{k\pm} : \phi = x, y\}$. A normal versor with

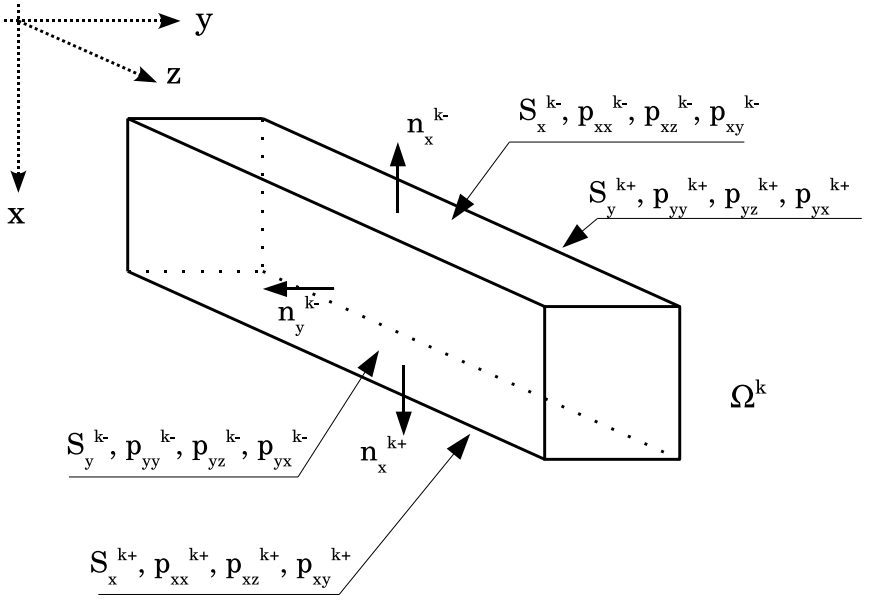


Fig. 2. Components of a surface loading lateral surfaces and normal vectors of the beam.

the same orientation as $x$ or $y$ axis identifies a positive lateral surface. The external virtual work due to $\mathbf{p}$ is

$$\delta L_p = \left(\delta L^k_{p^{\pm}_{xx}} + \delta L^k_{p^{\pm}_{yy}} + \delta L^k_{p^{\pm}_{xz}} + \delta L^k_{p^{\pm}_{yz}} + \delta L^k_{p^{\pm}_{xy}} + \delta L^k_{p^{\pm}_{yx}}\right)_k. \tag{4.9}$$

Its explicit terms are

$$\begin{aligned}
\left(\delta L^k_{p^{\pm}_{xx}}, \delta L^k_{p^{\pm}_{yx}}\right) &= \int_l \delta u_{x\tau}(p^{k\pm}_{xx} E^{ky^{\pm}}_{\tau}, p^{k\pm}_{yx} E^{kx^{\pm}}_{\tau})\, dz,\\
\left(\delta L^k_{p^{\pm}_{yy}}, \delta L^k_{p^{\pm}_{xy}}\right) &= \int_l \delta u_{y\tau}(p^{k\pm}_{yy} E^{kx^{\pm}}_{\tau}, p^{k\pm}_{xy} E^{ky^{\pm}}_{\tau})\, dz,\\
\left(\delta L^k_{p^{\pm}_{xz}}, \delta L^k_{p^{\pm}_{yz}}\right) &= \int_l \delta u_{z\tau}(p^{k\pm}_{xz} E^{ky^{\pm}}_{\tau}, p^{k\pm}_{yz} E^{kx^{\pm}}_{\tau})\, dz,
\end{aligned} \tag{4.10}$$

where

$$\begin{aligned}
(E^{kx^+}_{\tau}, E^{kx^-}_{\tau}) &= \int_{x^k_1}^{x^k_2} (F_\tau(x, y^k_2), F_\tau(x, y^k_1))\, dx,\\
(E^{ky^+}_{\tau}, E^{ky^-}_{\tau}) &= \int_{y^k_1}^{y^k_2} (F_\tau(x^k_2, y), F_\tau(x^k_1, y))\, dy.
\end{aligned} \tag{4.11}$$

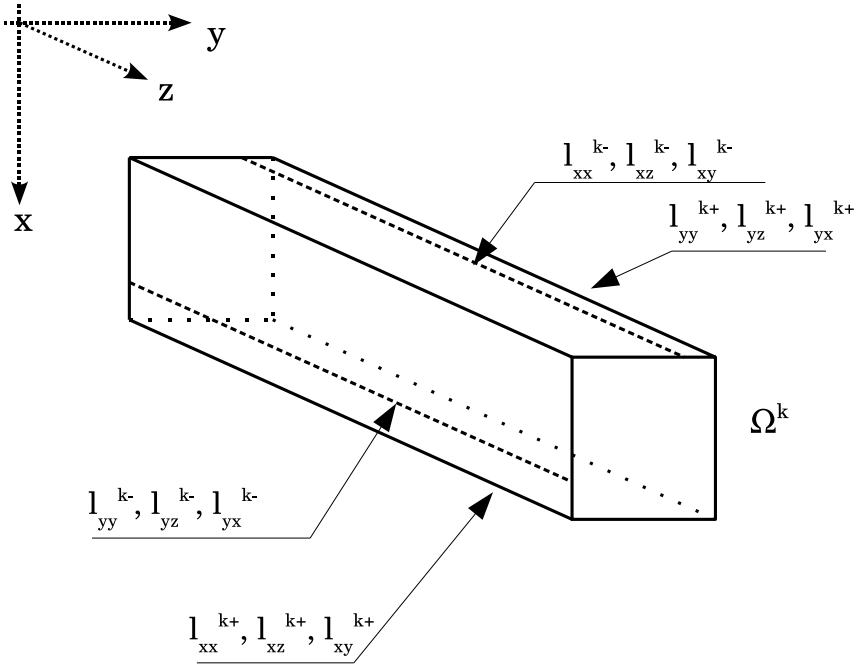


Fig. 3. Components of a line loading.

The closed form solution of the integrals in Eqs. (4.11) is presented in appendix B.

4.2.2. *Line loading*

The components of a line loading (see Fig. 3) are

$$\mathbf{l}^{kT} = \{l^{k\pm}_{xx} \quad l^{k\pm}_{yy} \quad l^{k\pm}_{xy} \quad l^{k\pm}_{yx} \quad l^{k\pm}_{xz} \quad l^{k\pm}_{yz}\}. \tag{4.12}$$

The external virtual work is

$$\delta L_l = \left(\delta L^k_{l^{\pm}_{xx}} + \delta L^k_{l^{\pm}_{yy}} + \delta L^k_{l^{\pm}_{xz}} + \delta L^k_{l^{\pm}_{yz}} + \delta L^k_{l^{\pm}_{xy}} + \delta L^k_{l^{\pm}_{yx}}\right)_k, \tag{4.13}$$

whose terms are

$$\begin{aligned}
(\delta L^k_{l^{\pm}_{xx}}, \delta L^k_{l^{\pm}_{yx}}) &= \int_l \delta u_{x\tau}(l^{k\pm}_{xx} F_\tau(x^k_{l^{\pm}_{xx}}, y^k_{l^{\pm}_{xx}}), l^{k\pm}_{yx} F_\tau(x^k_{l^{\pm}_{yx}}, y^k_{l^{\pm}_{yx}}))\, dz,\\
(\delta L^k_{l^{\pm}_{yy}}, \delta L^k_{l^{\pm}_{xy}}) &= \int_l \delta u_{y\tau}(l^{k\pm}_{yy} F_\tau(x^k_{l^{\pm}_{yy}}, y^k_{l^{\pm}_{yy}}), l^{k\pm}_{xy} F_\tau(x^k_{l^{\pm}_{xy}}, y^k_{l^{\pm}_{xy}}))\, dz,\\
(\delta L^k_{l^{\pm}_{xz}}, \delta L^k_{l^{\pm}_{yz}}) &= \int_l \delta u_{z\tau}(l^{k\pm}_{xz} F_\tau(x^k_{l^{\pm}_{xz}}, y^k_{l^{\pm}_{xz}}), l^{k\pm}_{yz} F_\tau(x^k_{l^{\pm}_{yz}}, y^k_{l^{\pm}_{yz}}))\, dz,
\end{aligned} \tag{4.14}$$

where $\{(x^k_{l^\pm_{ij}}, y^k_{l^\pm_{ij}}) : i = x, y; j = x, y, z\}$ are the coordinates of the line loading application point above a $k$ cross-section sub-domain.

### 4.3. *The fundamental nucleo*

The explicit form of the fundamental nucleo of the governing equations is obtained form Eqs. (4.5), (4.10) and (4.14)

$$
\begin{aligned}
\delta u_{x\tau}: \quad & (C_{11}E_{\tau,_x s,_x} + C_{66}E_{\tau,_y s,_y})u_{xs} - C_{55}E_{\tau s}u_{xs,_{zz}} \\
& + (C_{12}E_{\tau,_x s,_y} + C_{66}E_{\tau,_y s,_x})u_{ys} + (C_{13}E_{\tau,_x s} - C_{55}E_{\tau s,_x})u_{zs,_z} \\
& = [p^{k\pm}_{xx}E^{ky^\pm}_{\tau} + p^{k\pm}_{yx}E^{kx^\pm}_{\tau} + l^{k\pm}_{xx}F_\tau(x^k_{l^\pm_{xx}}, y^k_{l^\pm_{xx}}) + l^{k\pm}_{yx}F_\tau(x^k_{l^\pm_{yx}}, y^k_{l^\pm_{yx}})]_k, \\
\delta u_{y\tau}: \quad & (C_{12}E_{\tau,_y s,_x} + C_{66}E_{\tau,_x s,_y})u_{xs} + (C_{22}E_{\tau,_y s,_y} + C_{66}E_{\tau,_x s,_x})u_{ys} \\
& - C_{44}E_{\tau s}u_{ys,_{zz}} + (C_{23}E_{\tau,_y s} - C_{44}E_{\tau s,_y})u_{zs,_z} \\
& = [p^{k\pm}_{yy}E^{kx^\pm}_{\tau} + p^{k\pm}_{xy}E^{ky^\pm}_{\tau} + l^{k\pm}_{yy}F_\tau(x^k_{l^\pm_{yy}}, y^k_{l^\pm_{yy}}) + l^{k\pm}_{xy}F_\tau(x^k_{l^\pm_{xy}}, y^k_{l^\pm_{xy}})]_k, \\
\delta u_{z\tau}: \quad & -(C_{13}E_{\tau s,_x} - C_{55}E_{\tau,_x s})u_{xs,_z} - (C_{23}E_{\tau s,_y} - C_{44}E_{\tau,_y s})u_{ys,_z} \\
& + (C_{44}E_{\tau,_y s,_y} + C_{55}E_{\tau,_x s,_x})u_{zs} - C_{33}E_{\tau s}u_{zs,_{zz}} \\
& = [p^{k\pm}_{xz}E^{ky^\pm}_{\tau} + p^{k\pm}_{yz}E^{kx^\pm}_{\tau} + l^{k\pm}_{xz}F_\tau(x^k_{l^\pm_{xz}}, y^k_{l^\pm_{xz}}) + l^{k\pm}_{yz}F_\tau(x^k_{l^\pm_{yz}}, y^k_{l^\pm_{yz}})]_k.
\end{aligned}
\tag{4.15}
$$

The boundary conditions are

$$
\begin{aligned}
[\delta u_{x\tau}C_{55}(E_{\tau s}u_{xs,_z} + E_{\tau s,_x}u_{zs})]^{z=l}_{z=0} = 0, \\
[\delta u_{y\tau}C_{44}(E_{\tau s}u_{ys,_z} + E_{\tau s,_y}u_{zs})]^{z=l}_{z=0} = 0, \\
[\delta u_{z\tau}(C_{13}E_{\tau s,_x}u_{xs} + C_{23}E_{\tau s,_y}u_{ys} + C_{33}E_{\tau s}u_{zs,_z})]^{z=l}_{z=0} = 0.
\end{aligned}
\tag{4.16}
$$

For a fixed approximation order, the nucleo has to be expanded versus the indexes $\tau$ and $s$ in order to obtain the governing equations and the boundary conditions that concern the desired model.

## 5. Closed Form Analytical Solution

The differential equations in Eqs. (4.15) and the related boundary conditions in Eqs. (4.16) are solved via a Navier type solution by adopting the following displacement field

$$
\begin{aligned}
u_{x\tau} &= U_{x\tau}F_\tau(x, y)\sin(\alpha z), \\
u_{y\tau} &= U_{y\tau}F_\tau(x, y)\sin(\alpha z), \\
u_{z\tau} &= U_{z\tau}F_\tau(x, y)\cos(\alpha z),
\end{aligned}
\tag{5.1}
$$

upon the assumption that the external loadings vary towards $z$ in the following manner

$$\mathbf{p}^k = \begin{Bmatrix} P_{xx}^{k\pm}\sin(\alpha z) \\ P_{yy}^{k\pm}\sin(\alpha z) \\ P_{xy}^{k\pm}\sin(\alpha z) \\ P_{yx}^{k\pm}\sin(\alpha z) \\ P_{xz}^{k\pm}\cos(\alpha z) \\ P_{yz}^{k\pm}\cos(\alpha z) \end{Bmatrix}, \quad \mathbf{l}^k = \begin{Bmatrix} L_{xx}^{k\pm}\sin(\alpha z) \\ L_{yy}^{k\pm}\sin(\alpha z) \\ L_{xy}^{k\pm}\sin(\alpha z) \\ L_{yx}^{k\pm}\sin(\alpha z) \\ L_{xz}^{k\pm}\cos(\alpha z) \\ L_{yz}^{k\pm}\cos(\alpha z) \end{Bmatrix}. \tag{5.2}$$

This last assumption does not represent a loss in generality, since a generic loading can be approximated via its Fourier's series expansion (see [Carrera and Giunta, 2007 and 2008]). Term $\alpha$ is

$$\alpha = \frac{m\pi}{l}, \tag{5.3}$$

where $m$ represents the half-wave number along the beam axis. $\{U_{i\tau} : i = x, y, z\}$ are the maximal amplitudes of the displacement components and $\{P_{i,j}^{k\pm} : i = x, y;\ j = x, y, z\}$ and $\{L_{i,j}^{k\pm} : i = x, y;\ j = x, y, z\}$ the maximal amplitudes of the surface and line loading, respectively. The displacement field in Eqs. (5.1) satisfies the boundary conditions, Eqs. (4.16), since

$$\begin{aligned} u_{x\tau}(0) &= u_{x\tau}(l) = 0, \\ u_{y\tau}(0) &= u_{y\tau}(l) = 0, \\ u_{z\tau,_z}(0) &= u_{z\tau,_z}(l) = 0. \end{aligned} \tag{5.4}$$

The fundamental algebraic nucleo is obtained from Eqs. (4.15) upon substitution of Eqs. (5.1) and (5.2)

$$\begin{aligned} \delta U_{x\tau}: \quad & (C_{11}E_{\tau,_x s,_x} + C_{66}E_{\tau,_y s,_y} + \alpha^2 C_{55}E_{\tau s})U_{xs} \\ & + (C_{12}E_{\tau,_x s,_y} + C_{66}E_{\tau,_y s,_x})U_{ys} - \alpha(C_{13}E_{\tau,_x s} - C_{55}E_{\tau s,_x})U_{zs} \\ & = [P_{xx}^{k\pm}E_\tau^{ky^\pm} + P_{yx}^{k\pm}E_\tau^{kx^\pm} + L_{xx}^{k\pm}F_\tau(x_{l_{xx}^\pm}^k, y_{l_{xx}^\pm}^k) + L_{yx}^{k\pm}F_\tau(x_{l_{yx}^\pm}^k, y_{l_{yx}^\pm}^k)]_k, \\ \delta U_{y\tau}: \quad & (C_{12}E_{\tau,_y s,_x} + C_{66}E_{\tau,_x s,_y})U_{xs} + (C_{22}E_{\tau,_y s,_y} + C_{66}E_{\tau,_x s,_x} \\ & + \alpha^2 C_{44}E_{\tau s})U_{ys} - \alpha(C_{23}E_{\tau,_y s} - C_{44}E_{\tau s,_y})U_{zs} \\ & = [P_{yy}^{k\pm}E_\tau^{kx^\pm} + P_{xy}^{k\pm}E_\tau^{ky^\pm} + L_{yy}^{k\pm}F_\tau(x_{l_{yy}^\pm}^k, y_{l_{yy}^\pm}^k) + L_{xy}^{k\pm}F_\tau(x_{l_{xy}^\pm}^k, y_{l_{xy}^\pm}^k)]_k, \\ \delta U_{z\tau}: \quad & -\alpha(C_{13}E_{\tau s,_x} - C_{55}E_{\tau,_x s})U_{xs} - \alpha(C_{23}E_{\tau s,_y} - C_{44}E_{\tau,_y s})U_{ys} \\ & + (C_{44}E_{\tau,_y s,_y} + C_{55}E_{\tau,_x s,_x} + \alpha^2 C_{33}E_{\tau s})U_{zs} \\ & = [P_{xz}^{k\pm}E_\tau^{ky^\pm} + P_{yz}^{k\pm}E_\tau^{kx^\pm} + L_{xz}^{k\pm}F_\tau(x_{l_{xz}^\pm}^k, y_{l_{xz}^\pm}^k) + L_{yz}^{k\pm}F_\tau(x_{l_{yz}^\pm}^k, y_{l_{xz}^\pm}^k)]_k. \end{aligned} \tag{5.5}$$

For a fixed approximation order, the algebraic system has to be assembled according to the summation indexes $\tau$ and $s$. Its solution yields the maximal displacement amplitudes. The strains are retrieved by the geometric relations, Eqs. (2.10), and the stresses via the generalised Hooke law, Eqs. (2.7).

## 6. Numerical Results and Discussion

Rectangular or I-shaped cross-sections are considered. A typical aluminium alloy is adopted. The mechanical properties are: Young's modulus, $E = 71700$ MPa, Poisson's ratio, $\nu = 0.30$. The beams are subjected to bending and torsional loadings. The half-wave number is equal to the unit. The results are validated towards elasticity solutions or three-dimensional FEM models.

### 6.1. *Rectangular cross-section*

A simply supported beam undergoing a bending loading of maximal amplitude $P_{xx}^{1+}$ is first investigated. The problem was solved by Timoshenko and Goodier [1970] under the hypothesis plane stress. The stress components $\sigma_{zz}$, $\sigma_{xx}$ and $\sigma_{xz}$ were written in terms of a stress function. The indefinite equilibrium equations were then reduced in terms of this stress function and solved. This solution is addressed here as 'TGB'. The span-to-height ratio, $l/a$, is assumed to be as high as 100 and as low as two. A rectangular section is adopted. The aspect ratio $a/b$ is assumed equal to 100. The stress components are put into a non-dimensionalised form according to the following formulas

$$\sigma_{zz}^{*} = \frac{\pi^2}{6}\frac{a^2}{l^2}\frac{\sigma_{zz}}{P_{xx}^{1+}}, \quad \sigma_{xx}^{*} = \frac{\sigma_{xx}}{P_{xx}^{1+}}, \quad \sigma_{xz}^{*} = \frac{2\pi}{3}\frac{a}{l}\frac{\sigma_{xz}}{P_{xx}^{1+}}. \tag{6.1}$$

They are all evaluated at $y = 0$. In the case of $\sigma_{zz}^{*}$ and $\sigma_{xx}^{*}$, $z$ equals $l/2$, while for $\sigma_{xz}^{*}$, $z = 0$. Several values of the $x$ coordinate are considered. Tables 2 and 3 present stresses for $l/a = 100$ and $l/a = 50$. Since bending mechanics is predominant, the proposed theories all accurately predict the bending stress $\sigma_{zz}^{*}$. The first-order

Table 2. Stress components for the rectangular cross-section under bending loading, $l/a = 100$.

| | $\sigma_{zz}^{*}$ | | $\sigma_{xx}^{*}$ | | $\sigma_{xz}^{*}$ | |
|---|---|---|---|---|---|---|
| TGB | 1.0000[a] | −1.0000[b] | 0.5000[c] | 1.0000[a] | 1.0000[c] | 0.0000[a] |
| $N = 4$ | 1.0000 | −1.0000 | 0.5000 | 1.0000 | 1.0000 | 0.0000 |
| $N = 3$ | 1.0000 | −1.0000 | 0.5000 | 1.2327 | 1.0000 | 0.0000 |
| $N = 2$ | 1.0000 | −1.0000 | 0.5000 | 1.0115 | 0.7051 | 0.5898 |
| $N = 1$ | 1.0000 | −1.0000 | 0.5238 | 0.5238 | 0.6667 | 0.6667 |
| TB | 1.0000 | −1.0000 | —[d] | — | 0.6667 | 0.6667 |
| EB | 1.0000 | −1.0000 | — | — | — | — |

Stresses evaluated at (a) $x = a/2$, (b) $x = -a/2$, (c) $x = 0$.
(d) Result not provided by the theory.

Table 3. Stress components for the rectangular cross-section under bending loading, $l/a = 50$.

| | $\sigma^*_{zz}$ | | $\sigma^*_{xx}$ | | $\sigma^*_{xz}$ | |
|---|---|---|---|---|---|---|
| TGB | 1.0001[a] | −1.0001[b] | 0.5000[c] | 1.0000[a] | 1.0000[c] | 0.0000[a] |
| $N = 4$ | 1.0001 | −1.0001 | 0.5000 | 1.0000 | 1.0000 | 0.0000 |
| $N = 3$ | 1.0002 | −1.0002 | 0.5000 | 1.2327 | 1.0000 | 0.0000 |
| $N = 2$ | 1.0000 | −1.0000 | 0.5000 | 1.0116 | 0.7051 | 0.5898 |
| $N = 1$ | 1.0000 | −1.0001 | 0.5237 | 0.5237 | 0.6667 | 0.6669 |
| TB | 1.0000 | −1.0000 | —[d] | — | 0.6667 | 0.6667 |
| EB | 1.0000 | −1.0000 | — | — | — | — |

Stresses evaluated at (a) $x = a/2$, (b) $x = -a/2$, (c) $x = 0$.
(d) Result not provided by the theory.

approximation yields a constant stress component $\sigma^*_{xx}$. The third-order model accurately describes the transverse shear stress component, but it does not satisfy the boundary condition for the case of $\sigma^*_{xx}$. In this last case, the fourth-order is required in order to match the reference solution. Figures 4 (a) to 4(c) present the variation in the stress components versus $x/a$ for $l/a \geq 100$. The theories all match the exact

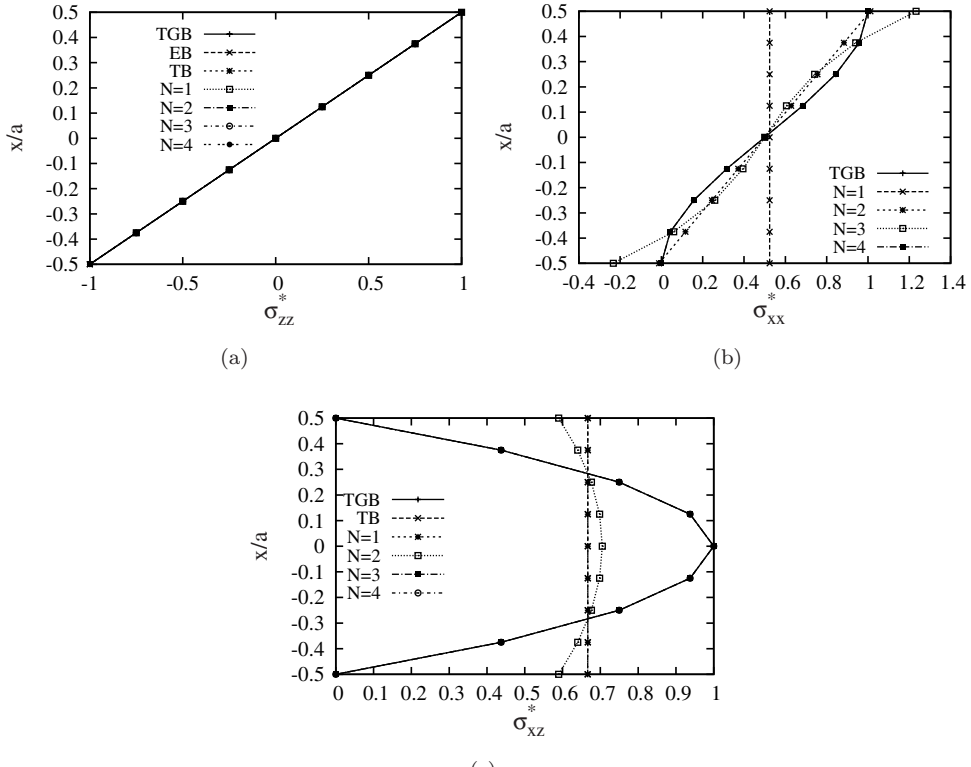


Fig. 4. (a) $\sigma^*_{zz}$, (b) $\sigma^*_{xx}$ and (c) $\sigma^*_{xz}$ versus $x/a$ for $l/a \geq 100$, bending loading and rectangular cross-section.

Table 4. Stress components for the rectangular cross-section under bending loading, $l/a = 10$.

| | $\sigma^*_{zz}$ | | $\sigma^*_{xx}$ | | $\sigma^*_{xz}$ | |
|---|---|---|---|---|---|---|
| TGB | 1.0034[a] | −1.0032[b] | 0.5000[c] | 1.0000[a] | 0.9992[c] | 0.0000[a] |
| $N = 5$ | 1.0034 | −1.0032 | 0.5000 | 1.0000 | 0.9992 | 0.0000 |
| $N = 4$ | 1.0034 | −1.0032 | 0.5000 | 1.0000 | 0.9994 | 0.0006 |
| $N = 3$ | 1.0052 | −1.0050 | 0.5000 | 1.2327 | 0.9993 | 0.0015 |
| $N = 2$ | 1.0000 | −1.0000 | 0.4988 | 1.0136 | 0.7040 | 0.5919 |
| $N = 1$ | 0.9962 | −1.0038 | 0.5221 | 0.5221 | 0.6667 | 0.6733 |
| TB | 1.0000 | −1.0000 | —[d] | — | 0.6667 | 0.6667 |
| EB | 1.0000 | −1.0000 | — | — | — | — |

Stresses evaluated at (a) $x = a/2$, (b) $x = -a/2$, (c) $x = 0$.
(d) Result not provided by the theory.

solution in the case of $\sigma^*_{zz}$. The third-order model yields a boundary value of $\sigma^*_{xx}$ that is worse than that computed via the second-order one. Table 4 presents the results regarding the case in which $l/a$ is equal to ten. $\sigma^*_{zz}$ is no longer symmetric versus the $x$ axis. An expansion order as high as five is required to match the exact solution up to the fifth significant digit. The fourth-order model is also very accurate. The results for $l/a$ equal to five are presented in Table 5. An accuracy of the first five significant digits calls for the sixth-order approximation. The fourth-order model is also accurate. The results regarding the case in which $l/a$ equals two are presented in Table 6. The higher order effects become relevant since the problem is governed by three-dimensional mechanics. Figures 5 (a) to 5(c) present the variation of the stress components above the cross-section. The stress component $\sigma^*_{zz}$ is no longer linear.

In the second case, a torsional moment is applied to the beam by means of two line loadings of equal maximal amplitude $L^{3+}_{xx} = L^{1-}_{xx} = L_{xx}$, as shown in Fig. 6. Classical models, such as EB and TB, yield displacement, strain and stress fields equal to zero for any case in which the resultant of the external loadings is equal to zero, even though the resultant moment is not. This is due to the fact that the

Table 5. Stress components for the rectangular cross-section under bending loading, $l/a = 5$.

| | $\sigma^*_{zz}$ | | $\sigma^*_{xx}$ | | $\sigma^*_{xz}$ | |
|---|---|---|---|---|---|---|
| TGB | 1.0144[a] | −1.0123[b] | 0.4998[c] | 1.0000[a] | 0.9967[c] | 0.0000[a] |
| $N = 6$ | 1.0144 | −1.0123 | 0.4998 | 1.0000 | 0.9967 | 0.0000 |
| $N = 5$ | 1.0144 | −1.0123 | 0.4998 | 1.0006 | 0.9967 | 0.0000 |
| $N = 4$ | 1.0144 | −1.0123 | 0.4998 | 1.0002 | 0.9977 | 0.0027 |
| $N = 3$ | 1.0216 | −1.0194 | 0.4998 | 1.2328 | 0.9971 | 0.0062 |
| $N = 2$ | 1.0014 | −0.9986 | 0.4952 | 1.0194 | 0.7008 | 0.5989 |
| $N = 1$ | 0.9851 | −1.0149 | 0.5170 | 0.5170 | 0.6667 | 0.6928 |
| TB | 1.0000 | −1.0000 | —[d] | — | 0.6667 | 0.6667 |
| EB | 1.0000 | −1.0000 | — | — | — | — |

Stresses evaluated at (a) $x = a/2$, (b) $x = -a/2$, (c) $x = 0$.
(d) Result not provided by the theory.

Table 6. Stress components for the rectangular cross-section under bending loading, $l/a = 2$.

| | $\sigma^*_{zz}$ | | $\sigma^*_{xx}$ | | $\sigma^*_{xz}$ | |
|---|---|---|---|---|---|---|
| TGB | 1.1287[a] | −1.0511[b] | 0.4930[c] | 1.0000[a] | 0.9780[c] | 0.0000[a] |
| $N = 6$ | 1.1287 | −1.0511 | 0.4930 | 1.0000 | 0.9780 | 0.0000 |
| $N = 5$ | 1.1295 | −1.0519 | 0.4930 | 1.0043 | 0.9780 | 0.0006 |
| $N = 4$ | 1.1294 | −1.0504 | 0.4944 | 1.0043 | 0.9844 | 0.0189 |
| $N = 3$ | 1.1714 | −1.0939 | 0.4941 | 1.2328 | 0.9810 | 0.0518 |
| $N = 2$ | 1.0492 | −0.9507 | 0.4694 | 1.0500 | 0.6786 | 0.6625 |
| $N = 1$ | 0.9129 | −1.0871 | 0.4837 | 0.4837 | 0.6667 | 0.8197 |
| TB | 1.0000 | −1.0000 | —[d] | — | 0.6667 | 0.6667 |
| EB | 1.0000 | −1.0000 | — | — | — | — |

Stresses evaluated at (a) $x = a/2$, (b) $x = -a/2$, (c) $x = 0$.
(d) Result not provided by the theory.

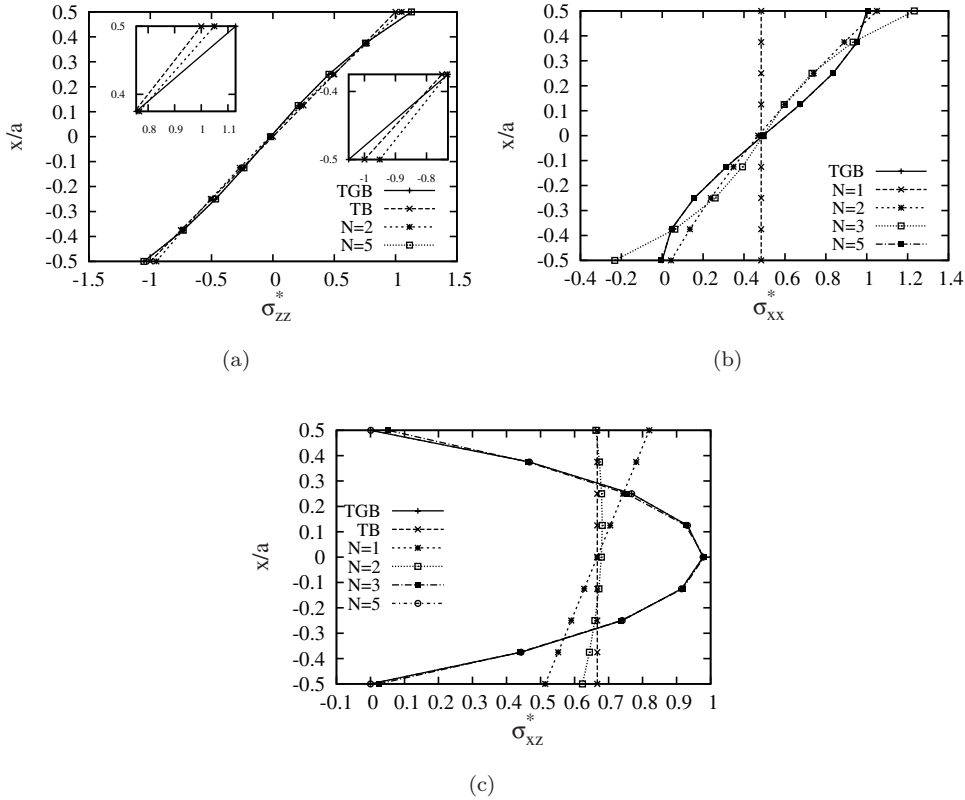


Fig. 5. (a) $\sigma^*_{zz}$, (b) $\sigma^*_{xx}$ and (c) $\sigma^*_{xz}$ versus $x/a$ for $l/a = 2$, bending loading and rectangular cross-section.

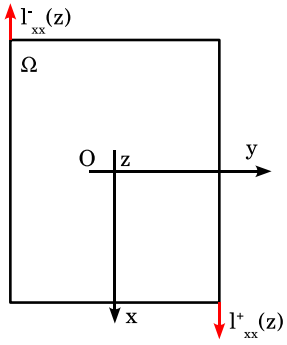


Fig. 6. Rectangular cross-section subjected to torsional loadings.

loadings coherent to these models are all applied to the section centroid. The first-order approximation does not yield the trivial solution, although the results may not be accurate. According to this model, the cross-section is too stiff on its plane. The following non-dimensionalised shear stress component $\sigma^*_{yz}$ is accounted for

$$\sigma^*_{yz} = \frac{ba^2}{M_t(z=0)}\sigma_{yz} = \pi\frac{a^2}{l}\frac{\sigma_{yz}}{L_{xx}}, \tag{6.2}$$

where $M_t(z=0)$ is the torsion moment at $z=0$. The shear stress component is evaluated at $2x/a=-1$ and $y=z=0$. The results are assessed towards the solution present in [Timoshenko and Goodier, 1970]. This solution is addressed as 'TGT' and it was obtained through Prandtl's membrane analogy. For a beam with a square cross-section, the reference solution is 4.807. This value does not depend upon the span-to-height ratio. The results are presented in Table 7 for an approximation order as high as 12 and several values of $l/a$. The twelfth-order approximation matches the reference solution for $l/a$ as low as 50. The two solutions differ by about 2.2%, in the case of $l/a=2$. In Table 8, the twelfth-order theory is compared to the reference solution. The aspect ratio is assumed as a free parameter. The span-to-height ratio ranges between 100 and two. The one-dimensional model matches the exact solution for $l/a$ as low as 50, the error being about 0.4%. For $l/a=5$ and $b/a=3$, the error is about 19%. In the case of $l/a=2$, it is equal to about 35%. It should be noticed that, in these cases, $l/b$ is 4/3 and one. The result for the cases

Table 7. $\sigma^*_{yz}$ versus $l/a$ for square cross-section and torsional loadings.

| $l/a$ | $\geq 50$ | 10 | 5 | 2 |
|---|---|---|---|---|
| $N=12$ | 4.807 | 4.804 | 4.796 | 4.700 |
| $N=9$ | 4.782 | 4.774 | 4.746 | 4.514 |
| $N=7$ | 4.858 | 4.857 | 4.853 | 4.784 |
| $N=5$ | 4.934 | 4.937 | 4.946 | 4.959 |
| $N=3$ | 3.000 | 2.996 | 2.985 | 2.877 |
| $N=1$ | 3.000 | 2.988 | 2.951 | 2.720 |

Table 8. $\sigma^*_{yz}$ versus the aspect ratio and $l/a$ via the twelfth-order approximation, rectangular cross-section and torsional loadings.

| $b/a$ | TGT | CUF, $N = 12$ | | | | |
|---|---|---|---|---|---|---|
| | | $l/a = 100$ | $l/a = 50$ | $l/a = 10$ | $l/a = 5$ | $l/a = 2$ |
| 1.5 | 4.329 | 4.329 | 4.328 | 4.291 | 4.178 | 3.533 |
| 2.0 | 4.065 | 4.064 | 4.062 | 3.979 | 3.740 | 2.619 |
| 3.0 | 3.745 | 3.737 | 3.730 | 3.533 | 3.018 | —[a] |

(a): $l/b < 1$.

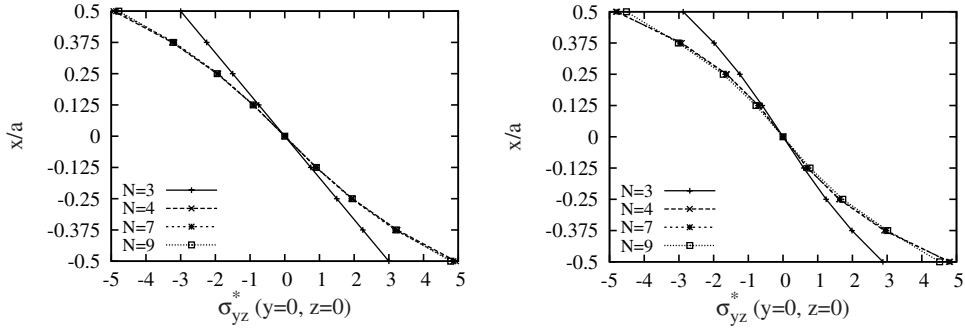


Fig. 7. $\sigma^*_{yz}$ versus $x/a$ for (a) $l/a \geq 50$ and (b) $l/a = 2$ in the case of square cross-section under torsional loadings.

$l/a = 2$ and $b/a = 3$ is not reported since $l/b$ becomes lower than unity and the structure is, therefore, no longer a beam. Figures 7(a) and 7(b) present the variation of $\sigma^*_{yz}$ towards $x/a$ for $l/a \geq 50$ and $l/a = 2$. A square cross-section is considered. Although the third-order approximation accounts for a cubic variation versus $x/a$, only the linear term is present for $l/a \geq 50$. The next relevant contribution is due to the fourth-order term. Fourth-, seventh- and ninth-order models can barely be distinguished. In the case of $l/a = 2$, the third-order term becomes relevant. In both cases, the main contribution to the solution is given by the fourth-order term. Figures 8(a) and 8(b) show the out-of-plane warping of the cross-section at $z = 0$ for $b/a = 3/2$ and $l/a = 100$ and two. The results are computed via the ninth-order approximation. The transverse displacement is non-dimensionalised with respect to the maximum value of the warping of an elliptic section of equal area and aspect ratio (see [Timoshenko and Goodier, 1970])

$$w^* = \frac{\pi}{L_{xx}} \frac{a^2 b}{l(b^2 - a^2)} \frac{E}{1+\nu} w. \tag{6.3}$$

Warping in the case of a rectangular cross-section is higher than that of the equivalent elliptic cross-section. As noted by Saint-Venant [1855], in the case of singly connected sections and for a given cross-sectional area, the lower the polar moment

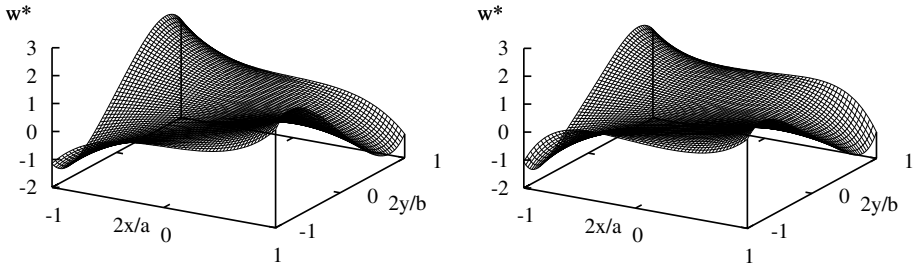


(a) (b)

Fig. 8. Transverse displacement $u_z^*$ versus $x/a$ and $y/b$ for (a) $l/a = 100$ and (b) $l/a = 2$ at $z = 0$ via the ninth-order approximation, rectangular cross-section ($b/a = 3/2$) under torsional loadings.

of inertia, the higher the torsional rigidity. Circular cross-sections yield the largest torsional rigidity and they do not present warping.

### 6.2. *I-shaped cross-section*

The cross-section geometry is such that $a/b = 3/2$ and $s_1/a = s_2/a = 1/4$. The span-to-height ratio is equal to 100 and ten. The beam undergoes bending or torsional loadings, as shown in Figs. 9(a) and 9(b). The loadings all have maximal amplitude equal to the unit. The maximum value and position of the displacement components are investigated. In the case of the bending loading, the displacement components are put into non-dimensionalised form as follows

$$(u^*_{x,\max}, u^*_{y,\max}, u^*_{z,\max}) = \frac{\pi^4}{12}\frac{a^3}{l^4}\frac{E}{P^{3+}_{xx}}(u_{x,\max}, u_{y,\max}, u_{z,\max}). \tag{6.4}$$

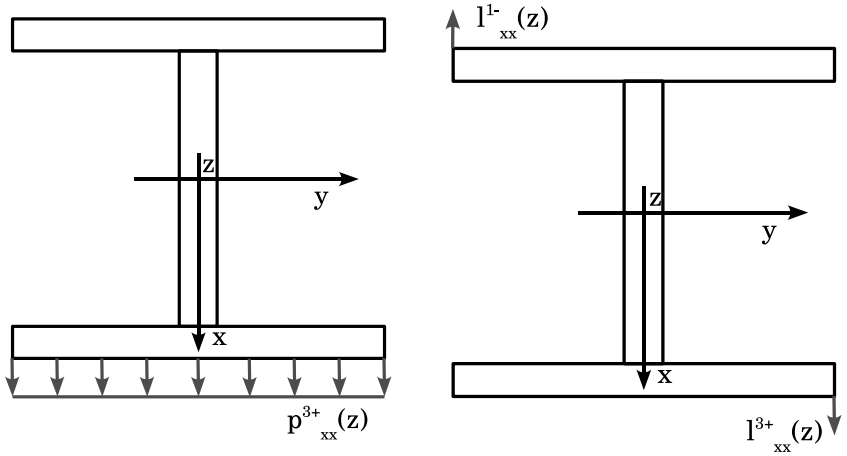


(a) (b)

Fig. 9. Loading configuration in the case of (a) bending or (b) torsional loadings, I-shaped cross-section.

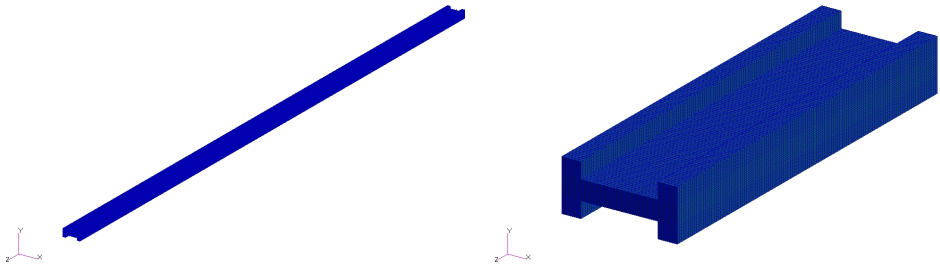

(a) (b)

Fig. 10. FEM models of the beams subjected to the surface loading. Due to the symmetry, only half of the structure is modelled.

Absolute values are considered for the case in which a displacement component presents an anti-symmetrical variation across the section. The solution to the problem via the proposed hierarchical models is compared to the three-dimensional FEM solution obtained via the MSC-Nastran commercial code. The eight-node "HEXA8" element is assumed. Due to problem symmetry versus the $z = l/2$ plane, half of the structure is analysed in the FEM model (see Figs. 10(a) and 10(b)). The mesh is such that $u_{x,\max}$ and $u_{z,\max}$ converged up to the first four digits and doubling the elements yields a lower change in $u_{y,\max}$ than 0.5%. In the case of the slender beam, 40000 solid elements are assumed, while for $l/a$ equal to ten, the number of elements is 115200. The results are presented in Table 9. The maximum approximation order is considered to be 18. In the case of slender beams, the maximum value of $u_x$ is at $x = 0$ and $y = \pm s_2$. The mechanics is governed by pure bending. The displacement component $u_y$ is anti-symmetrical towards the $x$-axis. The maximum of the

Table 9. Maximum displacements for the I-shaped cross-section subjected to bending loading.

| | $10 \times u^*_{x,\max}$ | $10^5 \times \lvert u^*_{y,\max}\rvert$ | $10^3 \times u^*_{z,\max}$ | $10 \times u^*_{x,\max}$ | $10^3 \times \lvert u^*_{y,\max}\rvert$ | $10^2 \times u^*_{z,\max}$ |
|---|---|---|---|---|---|---|
| | $l/a = 100$ | | | $l/a = 10$ | | |
| FEM 3D | 3.640[a] | 2.699[b] | 8.570[c] | 4.059[d] | 3.102[b] | 8.748[c] |
| $N = 18$ | 3.640 | 2.695 | 8.570 | 4.051 | 3.040 | 8.745 |
| $N = 10$ | 3.640 | 2.695 | 8.570 | 4.038 | 2.973 | 8.742 |
| $N = 9$ | 3.640 | 2.694 | 8.570 | 4.038 | 2.967 | 8.742 |
| $N = 8$ | 3.640 | 2.694 | 8.570 | 4.035 | 2.958 | 8.740 |
| $N = 7$ | 3.640 | 2.694 | 8.570 | 4.034 | 2.946 | 8.740 |
| $N = 6$ | 3.640 | 2.694 | 8.570 | 4.026 | 2.941 | 8.738 |
| $N = 5$ | 3.640 | 2.694 | 8.570 | 4.025 | 2.929 | 8.738 |
| $N = 4$ | 3.640 | 2.693 | 8.570 | 4.014 | 2.867 | 8.743 |
| $N = 3$ | 3.640 | 2.693 | 8.570 | 4.014 | 2.814 | 8.743 |
| $N = 2$ | 3.639 | 2.693 | 8.568 | 3.878 | 2.805 | 8.593 |
| $N = 1$ | 3.639[e] | 0.001[e] | 8.569[e] | 3.886[e] | 0.058[e] | 8.669[e] |
| TB | 3.639[f] | – | 8.568 | 3.881[f] | – | 8.568 |
| EB | 3.636[f] | – | 8.568 | 3.636[f] | – | 8.568 |

Maximum value at: (a) $(0, \pm s_2/2, l/2)$; (b) $(a/2 + s_1, \pm b/2, l/2)$; (c) $(-a/2 - s_1, 0, 0)$; (d) $(a/2, \pm b/2, l/2)$. (e) Maximum position different from the reference FEM solution. (f) The cross-section is rigid on its plane.

absolute value occurs at $x = a/2 + s_1$ and $y = \pm b/2$. This is due to Poisson effect. Both maximum values of $u_x$ and $u_y$ occur at $z = l/2$, according to Eqs. 5.1. The maximum value of $u_z$ is at $x = -(a/2 + s_1)$, $y = 0$ and $z = 0$. For $z = l$, there is the minimum of $u_z$. This displacement component does not present any symmetrical variation along the section although the mechanics is governed by bending. Classical models yield the same value of $u_{z,\max}$ as higher order theories do. The section is considered rigid on its plane. The Poisson effect is neglected. The first-order approximation accounts for it, but the section is still too stiff on its plane. At least the second-order terms are required. The first-order approximation does not yield the correct position of the maximum value of the displacements, although the values of $u_{x,\max}$ and $u_{z,\max}$ are close to those computed via higher order approximations. The analytical solution matches the FEM one. In the case of the span-to-height ratio equal to ten, the maximum values of $|u_y|$ and $u_z$ occur at the same locations as for the slender beam. The position of $u_{x,\max}$ changes. It is at $x = a/2$ and $y = \pm b/2$. It shifts towards the loading application area. As far as four significant digits are concerned, the convergence of $u_{z,\max}$ is obtained via the third-order approximation. Classical models yield a value that differs by about 2%. The maximum values of $u_x$ and $u_y$ present a slower convergence than $u_z$. This is more pronounced in the case of $u_y$, since it is due to the Poisson transverse contraction. The maximum value of $u_x$, computed via EB, differs by about 10% from the one obtained via the maximum approximation order. The difference is about 4% in the case of TB and second-order approximation. For approximation orders higher than the third-one, the even terms do not improve the value of $u_{x,\max}$ except for the fourth significant digit.

The results regarding the beam subjected to the torsional loadings are presented in Table 10. The maximum order of the approximation is considered to be 21. The

Table 10. Maximum displacements for the I-shaped cross-section subjected to torsional loadings.

| | $10^3 \times \lvert u^*_{x,\max}\rvert$ | $10^3 \times \lvert u^*_{y,\max}\rvert$ | $10^5 \times u^*_{z,\max}$ | $10 \times \lvert u^*_{x,\max}\rvert$ | $10 \times \lvert u^*_{y,\max}\rvert$ | $10^2 \times u^*_{z,\max}$ |
|---|---|---|---|---|---|---|
| | $l/a = 100$ | | | $l/a = 10$ | | |
| FEM 3D | 2.481[a] | 5.580[a] | 5.265[b] | 2.408[a] | 5.164[a] | 4.870[b] |
| $N = 21$ | 2.365 | 5.318 | 5.093 | 2.293 | 4.939 | 4.675 |
| $N = 20$ | 2.365 | 5.318 | 5.093 | 2.289 | 4.937 | 4.673 |
| $N = 19$ | 2.331 | 5.242 | 5.021 | 2.261 | 4.872 | 4.612 |
| $N = 10$ | 2.091 | 4.703 | 4.425 | 2.031 | 4.412 | 4.112 |
| $N = 9$ | 1.941 | 4.367 | 4.044 | 1.899 | 4.118 | 3.777 |
| $N = 8$ | 1.941 | 4.367 | 4.044 | 1.891 | 4.118 | 3.779 |
| $N = 7$ | 1.674 | 3.766 | 3.301[c] | 1.655 | 3.593 | 3.118[c] |
| $N = 6$ | 1.674 | 3.766 | 3.302[c] | 1.644 | 3.598 | 3.128[c] |
| $N = 5$ | 1.636 | 3.679 | 3.177[c] | 1.609 | 3.520 | 3.013[c] |
| $N = 4$ | 1.636 | 3.679 | 3.177[c] | 1.598 | 3.510 | 3.011[c] |
| $N = 3$ | 0.632 | 1.422 | 1.378[c] | 0.656 | 1.401 | 1.332[c] |
| $N = 2$ | 0.632 | 1.422 | 1.378[c] | 0.629 | 1.388 | 1.328[c] |
| $N = 1$ | 0.190 | 0.428 | 0.203[c] | 0.209 | 0.429 | 0.201[c] |

Maximum value at: (a) $(\pm(a/2+s_1), \pm b/2, l/2)$; (b) $(\pm a/2, \pm b/2, 0)$. (c) Maximum position different from the reference FEM solution.

following non-dimensionalised displacements are considered

$$(u^*_{x,\max}, u^*_{y,\max}, u^*_{z,\max}) = \frac{\pi^4}{12}\frac{a^3 b}{l^4}\frac{E}{L^+_{xx}}(u_{x,\max}, u_{y,\max}, u_{z,\max}). \tag{6.5}$$

FEM models have the same mesh as those developed for the solution of the previous problem. A further refinement of the mesh, by doubling the elements, yields a lower variation of the displacements than 0.5%. The maximum absolute values of the displacement components $u_x$ and $u_y$ occur at the points $\pm(a/2 + s_1, b/2, 0)$ for both values of the span-to-height ratio. The maximum value of $u_z$ is at $\pm(a/2, b/2)$ and $z = 0$. Its location is not correctly predicted by approximation orders as low as the seventh one. Due to the loading condition, the convergence is also slow in the case of the slender beam. Tenth- and 21st-order approximations at best differ by 11%. The FEM solution and maximum approximation orders that have been adopted differ by about 5% for both values of the span-to-height ratio. The solution above the whole cross-section may not always be accurately predicted via the information in a single point as theories based on Mac Laurin's polynomial functions are. For a fixed number of unknowns, the assumption of other polynomial approximations, such as the Lagrange ones, should be investigated. For higher approximation orders than the fourth one, the odd terms do not improve the results for slender beams. For $l/a$ equal to ten, only the fourth significant digit changes. The results may be improved by assuming higher approximation orders than those considered here. As far as the computational costs are concerned, the proposed analytical models require less than a second, regardless the approximation order. The FEM solution based on the proposed models, not reported here for sake of brevity, is obtained in few seconds for a very fine mesh. For the reference three-dimensional FEM solutions, more than two hours are required.

## 7. Conclusions

A unified formulation, named CUF, has been proposed for beam structures. Higher order models that account for shear deformations and in- and out-of-plane warping can be formulated straightforwardly. Within the proposed formulation, classical models, such as Euler-Bernoulli's and Timoshenko's, are regarded as particular cases. Closed form, Navier type solution for beams subjected to bending and torsional loadings has been addressed. Rectangular and I-shaped cross-sections have been considered. The following conclusions can be drawn:

(i) As far as bending loadings are concerned, the proposed formulation allows obtaining results as accurate as desired through an appropriate choice of the approximation order. The results of one-dimensional CUF models match the three-dimensional mechanics.

(ii) Classical models are accurate where the mechanics is governed by global bending, that is, for slender beams.

(iii) The first-order model can be regarded as a transition between classical models and refined theories since it accounts for non-classical effects although not accurately in the case of deep beams.
(iv) In the case of a deep beam with a rectangular cross-section, the sixth-order model matches the exact reference solution.
(v) Mechanics due to torsional loadings is more difficult to describe accurately. Higher approximation order than the bending case are required. The accuracy depends on the type of the cross-section, on the span-to-height ratio and on the aspect ratio.
(vi) Within CUF, the description of warping does not require any specific warping-function but it derives from the formulation itself.
(vii) The efficiency of the models is very high since the computational costs are of the order of $10^{-1}$ seconds, while the three-dimensional finite element models require about two hours.

The assumption of Lagrange's polynomials for the approximation above the cross-section represents an attractive solution to capture non classical, local phenomena on the cross-section. This will be the subject of further investigation together with the investigation of cross-section of aeronautical interest, such as wings and rotor blades' profiles.

**Acknowledgments**

Second author is supported by the Ministère de la Culture, de l'Enseignement Supérieuer et de la Recherche of Luxembourg under AFR-Postdoc grant TR-PDR BFR07-136.

## Appendix

### A. Correction of Poisson's Locking

The Poisson ratio couples the normal deformations along the spatial directions $x$, $y$, and $z$. Because of this, constant and linear approximations of the displacements do not yield accurate results, even in the case of slender beams. This phenomenon is known in literature as Poisson's Locking (PL). A modified version of material's constitutive equations, in which the stiffness coefficients are opportunely modified, should therefore be adopted. A correction of the PL is obtained imposing $\sigma_{xx}$ and $\sigma_{yy}$ equal to zero in Hooke's law. An algebraic linear system is obtained in $\epsilon_{xx}$ and $\epsilon_{yy}$. By substituting its solution in Hooke's equation regarding $\sigma_{zz}$, the reduced stiffness coefficient $Q_{33}$ is obtained

$$Q_{33} = C_{33} - C_{13}\frac{C_{23}C_{12} - C_{13}C_{22}}{C_{12}^2 - C_{11}C_{22}} + C_{23}\frac{C_{11}C_{23} - C_{12}C_{13}}{C_{12}^2 - C_{11}C_{22}} \tag{A.1}$$

In the case of isotropic materials

$$Q_{33} = E \tag{A.2}$$

## B. Analytical Integration over the Cross-Section

The closed form solution of the integrals in Eqs. (4.6), named the cross-section momenta, is presented for the case of a generic cross-section that can be obtained as union of rectangular sub-domains $\Omega^k$. Extension to generic quadrilateral sub-domains is straightforward via the assumption of a natural coordinates reference system. The generic function that has to be integrated is the product between $F_\tau = x^i y^j$ and $F_s = x^\eta y^\theta$ or their derivatives

$$E^k_{\tau,_x s,_x} = \frac{i\eta}{i+\eta-1}[(x_2^k)^{i+\eta-1} - (x_1^k)^{i+\eta-1}] \times \frac{1}{j+\theta+1}[(y_2^k)^{j+\theta+1} - (y_1^k)^{j+\theta+1}]. \tag{B.1}$$

$$E^k_{\tau,_y s,_y} = \frac{1}{i+\eta+1}[(x_2^k)^{i+\eta+1} - (x_1^k)^{i+\eta+1}] \times \frac{j\theta}{j+\theta-1}[(y_2^k)^{j+\theta-1} - (y_1^k)^{j+\theta-1}]. \tag{B.2}$$

$$E^k_{\tau s} = \frac{1}{i+\eta+1}[(x_2^k)^{i+\eta+1} - (x_1^k)^{i+\eta+1}] \times \frac{1}{j+\theta+1}[(y_2^k)^{j+\theta+1} - (y_1^k)^{j+\theta+1}]. \tag{B.3}$$

$$E^k_{\tau,_x s,_y} = \frac{\eta}{i+\eta}[(x_2^k)^{i+\eta} - (x_1^k)^{i+\eta}]\frac{j}{j+\theta}[(y_2^k)^{j+\theta} - (y_1^k)^{j+\theta}]. \tag{B.4}$$

$$E^k_{\tau,_y s,_x} = \frac{i}{i+\eta}[(x_2^k)^{i+\eta} - (x_1^k)^{i+\eta}]\frac{\theta}{j+\theta}[(y_2^k)^{j+\theta} - (y_1^k)^{j+\theta}]. \tag{B.5}$$

$$E^k_{\tau,_x s} = \frac{i}{i+\eta}[(x_2^k)^{i+\eta} - (x_1^k)^{i+\eta}]\frac{1}{j+\theta+1}[(y_2^k)^{j+\theta+1} - (y_1^k)^{j+\theta+1}]. \tag{B.6}$$

$$E^k_{\tau s,_x} = \frac{\eta}{i+\eta}[(x_2^k)^{i+\eta} - (x_1^k)^{i+\eta}]\frac{1}{j+\theta+1}[(y_2^k)^{j+\theta+1} - (y_1^k)^{j+\theta+1}]. \tag{B.7}$$

$$E^k_{\tau,_y s} = \frac{1}{i+\eta+1}[(x_2^k)^{i+\eta+1} - (x_1^k)^{i+\eta+1}]\frac{j}{j+\theta}[(y_2^k)^{j+\theta} - (y_1^k)^{j+\theta}]. \tag{B.8}$$

$$E^k_{\tau s,_y} = \frac{1}{i+\eta+1}[(x_2^k)^{i+\eta+1} - (x_1^k)^{i+\eta+1}]\frac{\theta}{j+\theta}[(y_2^k)^{j+\theta} - (y_1^k)^{j+\theta}]. \tag{B.9}$$

$$(E_\tau^{ky^+}, E_\tau^{ky^-}) = \frac{((x_2^k)^i, (x_1^k)^i)}{j+1}[(y_2^k)^{j+1} - (y_1^k)^{j+1}]. \tag{B.10}$$

$$(E_\tau^{kx^+}, E_\tau^{kx^-}) = \frac{((y_2^k)^j, (y_1^k)^j)}{i+1}[(x_2^k)^{i+1} - (x_1^k)^{i+1}]. \tag{B.11}$$

## References


Berdichevzy, V. L. [1976] "Equations of the theory of anisotropic inhomogeneous rods," *Doklady Akademii Nauk* SSR **228**, 558–561.

Carrera, E. [2003] "Theories and finite elements for multilayered plates and shells: A unified compact formulation with numerical assessment and benchmarking," *Archives of Computational Methods in Engineering* **10**(3), 215–296.

Carrera, E. and Giunta, G. [2007] "Hierarchical closed form solutions for plates bent by localized transverse loadings," *Journal of Zhejiang University SCIENCE A* **8**(7), 1026–1037.

Carrera, E. and Brischetto, S. [2008a] "Analysis of thickness locking in classical, refined and mixed multilayered plate theories," *Composite Structures* **82**(4), 549–562.

Carrera, E. and Brischetto, S. [2008b] "Analysis of thickness locking in classical, refined and mixed theories for layered shells," *Composite Structures* **85**(1), 83–90.

Carrera, E. and Giunta, G. [2008] "Hierarchical models for failure analysis of plates bent by distributed and localized transverse loadings," *Journal of Zhejiang University SCIENCE A* **9**(5), 600–613.

Cowper, G. R. [1966] "The shear co-efficient in Timoshenko beam theory," *Journal of Applied Mechanics* **33**(10), 335–340.

Estivalezes, E. and Barrau, J. J. [1998] "Analytical theory for an approach calculation of composite box beams subjected to tension and bending," *Composites Part B* **29**(4), 371–376.

Ganapathi, M., Patel, B. P., Polit, O. and Touratier, M. [1999] "A $C^1$ finite element including transverse shear and torsion warping for rectangular sandwich beams," *International Journal for Numerical Methods in Engineering* **45**(1), 47–75.

Gjelsvik, A. [1981] *The Theory of Thin-Walled Bars* (John Wiley and Sons, Inc., New York).

Hodges, D. H. [1990] "A review of composite rotor blade modeling," *AIAA Journal* **28**(3), 561–565.

Hodges, D. H. and Yu, W. [2007] "A rigorous, engineer-friendly approach for modelling realistic, composite rotor blades," *Wind Energy* **10**, 179–193.

Kant, T. and Manjunath, B. S. [1989] "Refined theories for composite and sandwich beams with $C^0$ finite elements," *Computers and Structures* **33**(3), 755–764.

Kant, T. and Manjunath, B. S. [1990] "Higher-order theories for symmetric and unsymmetric fiber reinforced composite beams with $C^0$ finite elements," *Finite Elements in Analysis and Design* **6**(4), 303–320.

Kapania, R. K. and Raciti, S. [1989a] "Recent Advances in Analysis of Laminated Beams and Plates, Part I: Shear Effects and Buckling," *AIAA Journal* **27**(7), 923–934.

Kapania, R. K. and Raciti, S. [1989b] "Recent Advances in Analysis of Laminated Beams and Plates, Part II: Vibrations and Wave Propagation," *AIAA Journal* **27**(7), 935–946.

Lee, J. and Lee, S. [2004] "Flexural-torsional behavior of thin-walled composite beams," *Thin-Walled Structures* **42**(9), 1293–1305.

Lee, J. [2005] "Flexural analysis of thin-walled composite beams using shear-deformable beam theory," *Composite Structures* **70**(2), 212–222.

Li, X. and Liu, D. [1997] "Generalized laminate theories based on double superposition hypothesis," *International Journal for Numerical Methods in Engineering* **40**(7), 1197–1212.

Liu, G. R. and Zhang, G. Y. [2009] "A novel scheme of strain-constructed point interpolation method for static and dynamic mechanics problems," *International Journal of Applied Mechanics* **1**(1), 233–258.

Manjunath, B. S. and Kant, T. [1993] "Different numerical techniques for the estimation of multiaxial stresses in symmetric/unsymmetric composite and sandwich beams with refined theories," *Journal of Reinforced Plastics and Composites* **12**(1), 2–37.

Murty, A. V. K. [1970] "Analysis of short beams," *AIAA Journal* **8**(11), 2098–2100.

Prandtl, L. [1903] "Zur Torsion von Prismatischen Stäben," *Zeitschrift Für Physik* **4**, 758–770.

Prathap, G. and Vinayak, R. U. and Naganarayana, B. P. [1996] "Beam elements based on a higher order theory - II. Boundary layer sensitivity and stress oscillations," *Computers and Structures* **58**(4), 791–796.

Rand, O. [1998] "Fundamental closed-form solutions for solid and thin-walled composite beams including a complete out-of-plane warping model," *International Journal of Solids and Structures* **35**(21), 2775–2793.

Rand, O. [2000] "On the importance of cross-sectional warping in solid composite beams," *Composite Structures* **49**(4), 393–397.

Reddy, J.-N. [2004] *Mechanics of laminated composite plates and shells. Theory and Analysis* (CRC Press).

Saint-Venant, B. [1855] "Memoire Sur la Torsion des Prismes," *Memoires des Savants Etrangers* **14**, 233–560.

Stephen, N. G. and Levinson, M. [1979] "A second order beam theory," *Journal of Sound and Vibration* **67**(3), 293–305.

Timoshenko, S. P. [1921] "On the corrections for shear of the differential equation for transverse vibrations of prismatic bars," *Philosophical Magazine* **41**, 744–746.

Timoshenko, S. P. [1922] "On the transverse vibrations of bars of uniform cross section," *Philosophical Magazine* **43**, 125–131.

Timoshenko, S. P. and Goodier, J.-N. [1970] *Theory of elasticity* (McGraw-Hill, New York).

Tsai, S. W. [1988] *Composites Design* (Dayton, Think Composites).

Vidal, P. and Polit O. [2008] "A family of sinus finite elements for the analysis of rectangular laminated beams," *Composite Structures* **84**(1), 56–72.

Vinayak, R. U. and Prathap, G. and Naganarayana, B. P. [1996] "Beam elements based on a higher order theory - I. Formulation and analysis of performance," *Computers and Structures* **58**(4), 775–789.

Yu, W. and Hodges, D. H. and Volovoi, V. and Cesnik, C. E. S. [2002] "On Timoshenko-like modeling of initially curved and twisted composites beams," *International Journal of Solids and Structures* **39**(19), 5101–5121.

Yu, W. and Hodges, D. H. [2004] "Elasticity solution versus asymptotic sectional analysis of homogeneous, isotropic, prismatic beams," *Journal of Applied Mechanics* **71**(1), 15–23.

Wagner, W. and Gruttmann, F. [2002] "A displacement method for the analysis of flexural shear stresses in thin-walled isotropic composite beams," *Computers Structures* **80**(24), 1843–1851.